IEEE Photonics Journal
An IEEE Photonics Society Publication

Experimental DCO-OFDM Optical Camera Communication Systems With a Commercial Smartphone Camera

Volume 11, Number 6, December 2019

Jenn-Kaie Lain, ***Member, IEEE***
Zheng-Dao Yang
Ting-Wei Xu

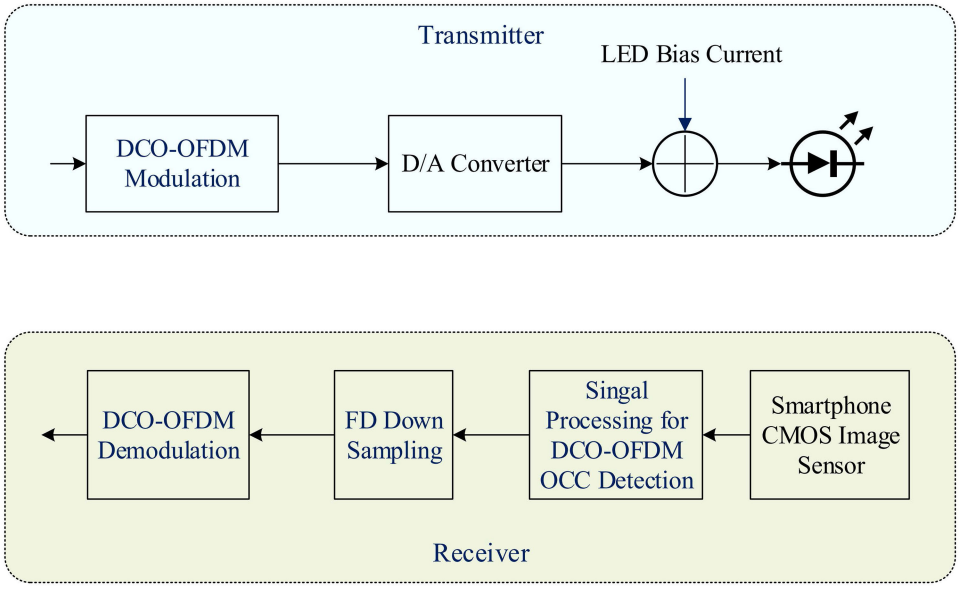

DOI: 10.1109/JPHOT.2019.2948071

IEEE photonics SOCIETY
IEEE

Experimental DCO-OFDM Optical Camera Communication Systems With a Commercial Smartphone Camera

Jenn-Kaie Lain, *Member, IEEE*, Zheng-Dao Yang, and Ting-Wei Xu

Department of Electronic Engineering, National Yunlin University of Science and Technology, Yunlin 64002, Taiwan

DOI:10.1109/JPHOT.2019.2948071

Manuscript received September 30, 2019; accepted October 14, 2019. Date of publication October 17, 2019; date of current version November 12, 2019. This work was supported by the Ministry of Science and Technology of Taiwan under Grant MOST-108-2221-E-224-018. Corresponding author: Jenn-Kaie Lain (e-mail: lainjk@yuntech.edu.tw).

Abstract: Modern handheld mobile devices are equipped with a complementary metal-oxide-semiconductor (CMOS) image sensor. These image sensors are capable of perceiving intensity changes in optically modulated signals, driving the rapid development of optical camera communication (OCC). In this study, direct-current offset orthogonal frequency division multiplexing (DCO-OFDM) was developed for a rolling shutter OCC system in order to improve the data transmission rates of OCC systems. Two DCO-OFDM OCC signal detection algorithms, namely the parabolic column vector selection (P-CVS) algorithm and the decomposition of extremely low frequency component (D-ELFC) algorithm, were proposed, along with a frequency-domain downsampling scheme, to eliminate the influence from both the blooming effect and shot noise. The experimental results, obtained after using a self-built DCO-OFDM OCC testbed with a general commercial smartphone camera, demonstrated that the D-ELFC algorithm outperformed in the bit error rate (BER) in comparison to the P-CVS algorithm and achieved a data transmission rate $>$22 kbps under the conditions of the BER being below the 20% forward error correction (FEC) limit and the illuminance being higher than 510 lux.

Index Terms: DCO-OFDM, LED, optical camera communications, optical wireless communications.

1. Introduction

Due to significant improvements in the technology used to manufacture light-emitting diodes (LEDs), the lighting cost per unit for LEDs has continued to decrease, prompting the LED to gradually become the mainstream form of indoor lighting. Visible light communication (VLC) uses LEDs to transmit optically modulated signals, and uses indoor lighting to achieve optical wireless communication to yield unified lighting and wireless communication systems [1], [2]. Initially, a VLC system uses a photodetector (PD) to transform the subtle variations in the intensity of an optically modulated signal into an electrical signal so that the receiver can demodulate the received signal. Recently, the cameras included in handheld mobile devices have generally been equipped with complementary metal-oxide-semiconductor (CMOS) image sensors, and these sensors have driven the rapid development of optical camera communication (OCC) [3], [4]. Currently, OCC technology has been incorporated into the IEEE 802. 15.7 m short range optical wireless communications specifications [5].

An OCC system uses a CMOS image sensor as an optical signal receiver. However, the main function of a CMOS image sensor is to take pictures and videos, and such sensors can typically only continuously capture images at a speed sufficient to achieve a smooth motion picture (video), generally 30 frames per second. In other words, the frame rate of current commercial CMOS image sensors is rather limited, resulting in a limitation in the data transmission rate of OCC systems utilizing such sensors. Therefore, the rolling shutter effect has recently been adopted to increase the data transmission rate of OCC systems [6]. However, it has remained difficult to increase such transmission rates significantly. At the same time, multiple input multiple output (MIMO), multilevel modulation, and multicarrier transmission techniques are considered to have the potential to improve OCC data transmission rates. Through the principle of spatial multiplexing, MIMO technology combines the independent data symbols from several LEDs into a coded image to improve OCC data transmission rates [7]. In this approach, a CMOS image sensor is regarded as a mass receiver. After receiving a coded image, the MIMO receiver has to estimate the channel state information for the purpose of signal demodulation, resulting in high computational complexity and high implementation costs. Multilevel intensity modulation (m-IM), in the form of pulse width modulation (PWM), has also been proposed as a means for improving OCC data transmission rates [8]. One OCC system utilizing 4-IM technology achieved a data rate of up to 10 kbps. However, to achieve higher data transmission rates, higher order IM signals would have to be employed, and the difficulty of demodulating such signals would make them unusable. Meanwhile, multi-carrier transmission is widely used in today's wireless communication systems. The use of orthogonal frequency division multiplexing (OFDM) transmission with a rolling shutter OCC system utilizing a commercial smartphone camera has great potential. The design and performance evaluation of the proposed novel OFDM OCC signal detection algorithms were carried out in the study to improve the data transmission rates of OCC systems.

Thus far, on-off keying (OOK) IM has been used in OCC systems utilizing the rolling shutter effect [9]–[12]. In this approach, when the shutter speed of the camera module is higher than the bit transmission rate, the OOK signal will be exposed row by row from top to bottom, so that the image sensor captures an image with dark and white fringes. These dark and white fringes represent the intensity variations of the transmitted optically modulated signal, and the image grayscale values are used to demodulate this information-bearing image into digital logical data. There has been little discussion of using OFDM transmission with an OCC system. In [13], two-dimensional OFDM (2D-OFDM) in screen OCC systems was proposed. However, the 2D-OFDM screen OCC transforms the data into coded images and requires the use of big screens to transmit these images. A quadrature phase shift keying direct-current offset OFDM (DCO-OFDM) OCC was implemented in the form of PWM using a spatial luminance distribution of two-dimensional LED image, in which a rolling shutter was not utilized [14]. But, the achieved data rate was quite limited because the transmitted symbol rate had to be lower than the image frame rate. In [15], theoretical and simulation results were given for the rolling OFDM OCC. However, there was limited information related to OFDM OCC signal detection, and the achieved data rate was around 2 kbps in the experimental results. DCO-OFDM also has previously been used in an OCC system [16]; however, that system uses a special optical communication image sensor, which has made it difficult to popularize. Therefore, the use of commercial image sensors built into general mobile devices for DCO-OFDM OCC signal demodulation was investigated in the present study in order to achieve the objective of low-cost and high-speed OCC transmission.

In this approach, the image sensor is basically used to receive the DCO-OFDM signal emitted by the LED, but the captured image is interfered with by blooming effect interference (BEI) and shot noise. Blooming is an effect that results when the charge developed on a pixel leaks into adjacent pixels and corrupts the scene, while shot noise is caused by the arrival process of light photons on the sensor. Since the OOK OCC system uses binary modulation signals, it has a certain degree of tolerance for shot noise that causes a short-term variation in the signal. However, BEI is mainly caused by the line-of-sight transmission from the LED, and consequently, it is a form of long-term interference that destroys the received image fringes. Relatedly, BEI is regarded as the main problem in OOK OCC signal demodulation. The OOK OCC literature explores the

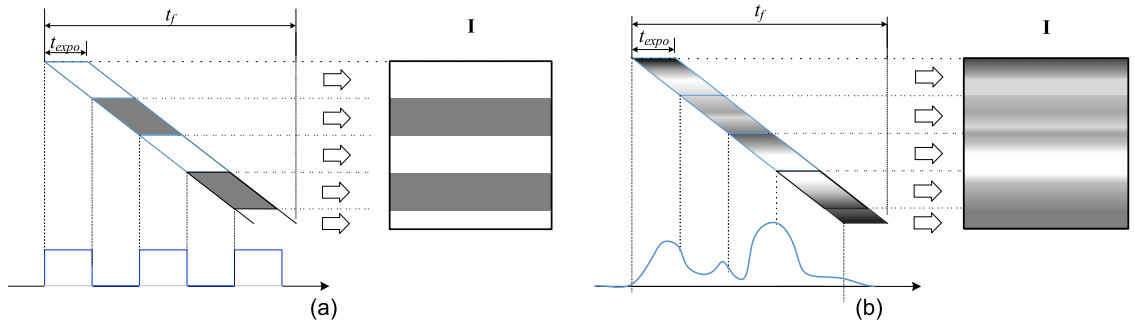

Fig. 1. Illustrations of the OCC system with (a) OOK modulation and (b) OFDM modulation.

use of different column vector selection (CVS) strategies to mitigate the effects of BEI on signal demodulation [9]–[12]. However, compared to the simple binary modulated signal used in OOK systems, the DCO-OFDM signal is analog, and performance degradation would be caused from signal distortion in the received DCO-OFDM samples. In this case, not only the long-term BEI, but also the short-term signal variation caused by the shot noise would have significant impacts on the performance of the DCO-OFDM OCC system. Therefore, in the present study, two DCO-OFDM OCC signal detection algorithms and a frequency-domain downsampling (FDDS) scheme were developed, and their performance was analyzed in an experimental testbed.

The remainder of this paper is organized as follows. Section 2 presents some preliminary work, with an emphasis on the operating principles of an OCC system and the DCO-OFDM OCC system modeling. The proposed DCO-OFDM OCC signal detection algorithms along with the FDDS scheme are detailed in Section 3. Section 4 describes the experimental setup and results. The conclusions are drawn in Section 5.

2. Preliminary

2.1 The Operating Principles of an OCC System

Fig. 1 illustrates the images that would be recorded by an image sensor in an OCC system when using OOK modulation and OFDM modulation. With the use of the rolling shutter, within a frame readout time t_f, the transmitted optically modulated signal is captured by horizontally scanning with an exposure time t_{expo} from top to bottom to form an image in RGB format. Owing to the use of IM, the received RGB image is transformed into grayscale format to retrieve its intensity information. Suppose the size of the grayscale image $\mathbf{I}$ is $I_H \times I_W$, where I_H and I_W denote the number of rows and the number of columns, respectively, and $I(i, j)$ is the pixel grayscale value of the i-th row and the j-th column in $\mathbf{I}$ with $1 \leq i \leq I_H$ and $1 \leq j \leq I_W$. Binary modulation was employed in traditional OOK OCC systems, and consequently, the captured image shows bright and dark fringes because the LED transmits only two kinds of light intensity, as shown in Fig. 1(a). The demodulation of the fringes embedded in the image, which are represented by grayscale values, back to logical bits was accomplished by constructing a column vector of grayscale values from the image frame and calculating a threshold function to decide the logical bits. In some previous studies, the polynomial fitting method was used for a grayscale column vector, which was selected based on various CVS methods, to calculate the threshold function to decide the logical bits [9]–[12].

An OCC system using OFDM modulation is considered in this paper. Using an inverse fast Fourier transform (IFFT), M-ary digital modulated symbols on each subcarrier are multiplexed to be a continuous time-domain signal, and then the resulting signal is superimposed onto a DC bias current to drive the LED. Consequently, the intensity of the LED is varied with the transmitted signal, and the greyscale values between the successive rows are continuously changing, as shown in Fig. 1(b), making such OFDM OCC different from the OOK OCC described above.

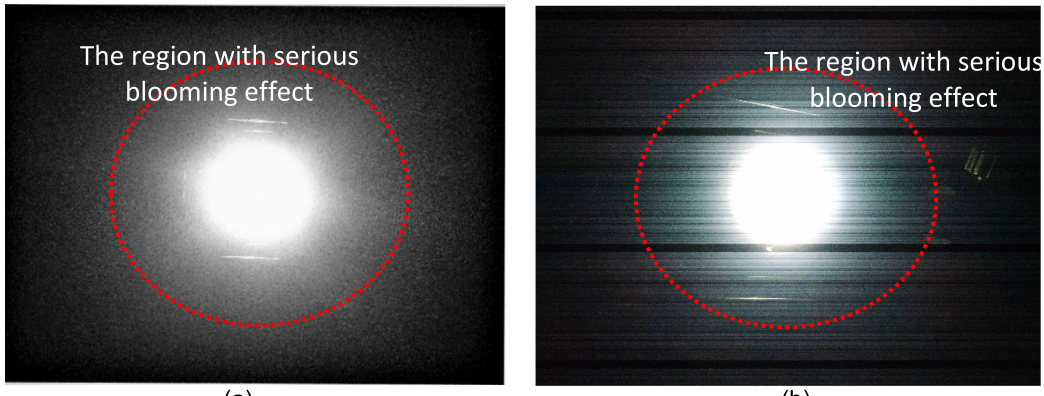

Fig. 2. LED images of 3492 × 4656 resolution: (a) without and (b) with the DCO-OFDM modulation signal.

Each time-domain OFDM sample is a composite of modulated symbols on all subcarriers, and thus the received signal distortion would cause serious performance degradation. In the approach proposed in this study, a commercial smartphone camera using a rolling shutter is employed to capture images of the LED that is driven and modulated by the DCO-OFDM signal. In addition to the intensity of the desired DCO-OFDM signal, the issues of BEI and shot noise during the process of optical-to-grayscale conversion are relevant factors. Using a commercial smartphone camera (ASUS ZE552KL), Fig. 2 shows images of the LED (Cree XPG2 R5) without and with the DCO-OFDM modulation signal. First of all, the tiny fringes in Fig. 2(b) are the result of changes in illuminance variation due to the DCO-OFDM modulation, while the pixels that are close to the center of the LED image are over-exposed. In addition, the charges on these pixels are totally saturated. As a result, it was not possible to record any changes in the grayscale values with these pixels. In addition, except for the blooming effect region, the grayscale value changes in the adjacent rows of the image are not obvious, showing a continuous variation characteristic of the received optical signal. In this situation, due to the small difference in the grayscale values of the adjacent rows of the image, the shot noise would apparently degrade the system performance.

2.2 DCO-OFDM OCC System Modeling

At a fixed symbol rate, DCO-OFDM has been considered to have lower computational complexity than asymmetrically clipped optical OFDM (ACO-OFDM) [17], so DCO-OFDM was adopted in this study. The block diagram of the DCO-OFDM OCC system is shown in Fig. 3, where $\mathbf{X} = [X_0, X_1, \ldots, X_n, \ldots, X_{N-1}]$ is the input signal of the DCO-OFDM modulation block, X_n is the M-ary quadrature amplitude modulated (QAM) complex data signal on the n-th subcarrier, and X_n in $\mathbf{X}$ must be Hermitian symmetric. Using the IFFT operation, $\mathbf{X}$ is converted into a bipolar and real time-domain signal $\mathbf{x} = [x_0, x_1, \ldots, x_{N-1}]$, where N is the size of the IFFT and the n-th time-domain sample in $\mathbf{x}$ is given by

$$x_n = \frac{1}{N} \sum_{k=0}^{N-1} X_k \exp\left(\frac{j2\pi nk}{N}\right). \tag{1}$$

To drive the LED to carry out the electrical-to-optical conversion, $\mathbf{x}$ must be added with a DC bias x_{DC} to have a positive DCO-OFDM signal $\mathbf{x}^{(DCO)} = [x_0^{(DCO)}, x_1^{(DCO)}, \ldots, x_{N-1}^{(DCO)}]$ [18], [19]. Signal $\mathbf{x}^{(DCO)}$ is then digital-to-analog (D/A) converted to a continuous electrical waveform $x(t)$. The LED serves as an optical modulator that transforms $x(t)$ into an optical signal, and the resulting signal is transmitted through the optical channel.

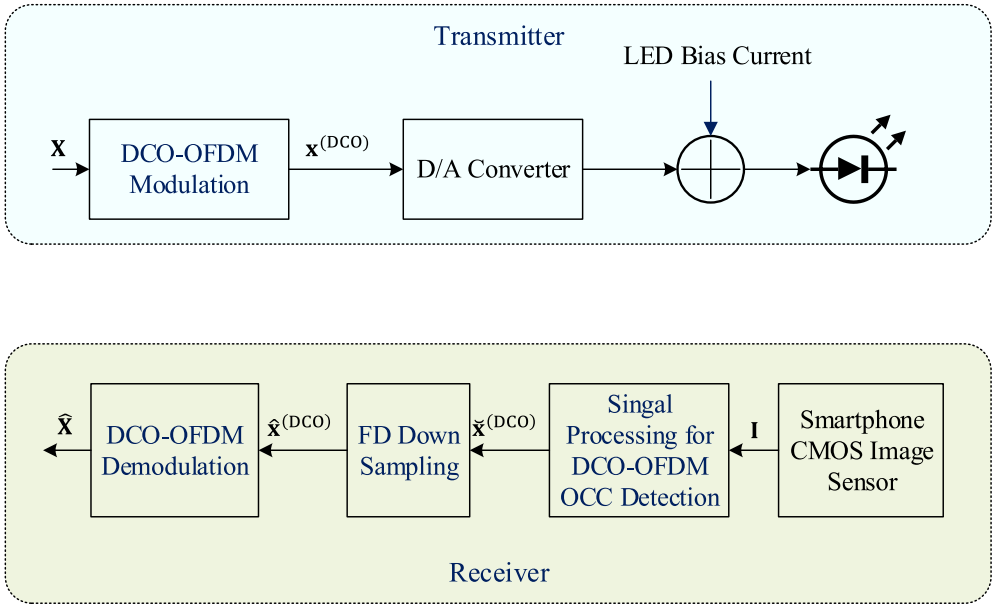

Fig. 3. DCO-OFDM OCC system block diagram.

The intensity of the modulated light is perceived by utilizing an embedded CMOS image sensor in a smartphone camera. The rolling shutter mechanism causes the intensity of the DCO-OFDM modulated signal from the captured videos or photos to be recorded in the grayscale value of each row of pixels. However, in addition to providing the desired DCO-OFDM modulated signal, the image is also interfered with by the shot noise $\mathbf{n}_{shot}$ and the BEI $\mathbf{n}_b$. Therefore, the pixel grayscale value $I(i, j)$ of the i-th row and the j-th column on the grayscale image $\mathbf{I}$ can be expressed as

$$I(i,j) = G_{og} \times G_{eo} \times x\left(i \cdot t_{expo}\right) + n_b(i,j) + n_{shot}(i,j), \tag{2}$$

where $1 \le i \le I_H$ and $1 \le j \le I_W$. G_{eo} and G_{og} are the electrical-to-optical gain of the LED and the optical-to-grayscale gain of the image sensor, respectively. $n_b(i, j) \in \mathbf{n}_b$ is the BEI of the i-th row and the j-th column pixel. $n_{shot}(i, j) \in \mathbf{n}_{shot}$ is the shot noise on the i-th row and the j-th column pixel that can be modeled as additive white Gaussian noise (AWGN) [20]. Based on Eq. (2), the effects of $\mathbf{n}_b$ and $\mathbf{n}_{shot}$ presented in $\mathbf{I}$ should be overcome to demodulate the DCO-OFDM OCC signal.

3. The Proposed DCO-OFDM OCC Signal Detection Algorithms

Fig. 3 consists of a block diagram of the DCO-OFDM OCC system using a commercial smartphone camera, in which two signal processing algorithms are proposed to reduce the influence of the BEI and the FDDS scheme is adopted to decrease the shot noise. Experimental implementation was carried out to evaluate and validate the proposed schemes for DCO-OFDM OCC signal detection.

3.1 The Parabolic Column Vector Selection Algorithm

Given a grayscale image $\mathbf{I}$, the DCO-OFDM OCC signal detection has to reduce the influence of the BEI $\mathbf{n}_b$ and the shot noise $\mathbf{n}_{shot}$ on $\mathbf{I}$ to get $\hat{\mathbf{x}}^{(DCO)}$, the estimation of $\mathbf{x}^{(DCO)}$. The proposed parabolic column vector selection (P-CVS) uses the sorted grayscale image and the grayscale column vector selection based on a parabolic equation to reduce the influence of $\mathbf{n}_b$. The image sorting was proposed for OOK OCC systems [11]. Fig. 4 shows the image that results from the sorting of each row in Fig. 2 in descending order and that is denoted as $\mathbf{I}_{sort}$. As seen in Fig. 4, the pixels in $\mathbf{I}_{sort}$ that experienced serious BEI are on the left side of $\mathbf{I}_{sort}$. Owing to the mechanism

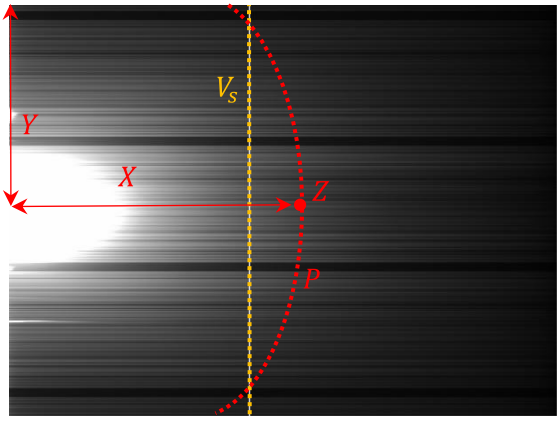

Fig. 4. Illustration of column vector selection methods.

of the rolling shutter, the transmitted DCO-OFDM signal is recorded as grayscale values on the image in a row-by-row and top-to-bottom manner, and hence a grayscale column vector should be formed from these grayscale values to serve as a replica of the received DCO-OFDM signal. In [11], two boundaries, B_l and B_r, in $\mathbf{I}_{sort}$ were used. B_l was used to prevent the selection of the pixels that were seriously damaged by the BEI, while B_r was applied to avoid picking the pixels that had insufficient exposure. Furthermore, the selected column vector V_s is an interpolation of B_l and B_r, and the orange dotted line in Fig. 4 represents the selected column vector with parameters that are the same as those in [11]. However, the grayscale values of the pixels, denoted as $\mathbf{G}_S$, on the selected column vector apparently suffer from different levels of BEI, which causes serious distortion of the received DCO-OFDM signal. Moreover, the settings of B_l and B_r can easily be affected by a variety of factors, including environmental lighting, the characteristics of the adopted image sensor, the adopted LED, etc. Thus, it is not easy to find a deterministic relationship through which to interpolate the V_s by using B_l and B_r.

In this study, we investigated how to reduce the influence of the BEI on the selected grayscale values, using a parabola to construct a grayscale column vector by selecting pixels from different columns in $\mathbf{I}_{sort}$. As can be seen in Fig. 4, the pixels that are closer to the center of the LED image are more damaged in terms of their grayscale values. Accordingly, the pixels on a specific column suffer from different levels of BEI. This motivated us to consider using a parabolic equation, denoted as the red dotted line in Fig. 4, to select pixels from different columns in $\mathbf{I}_{sort}$ that might experience almost the same levels of BEI. The coordinates (x, y) in the parabolic equation P are represented as follows,

$$P : y^2 = -2px, p \geq 0, \tag{3}$$

where $1/p$ denotes the maximum curvature of the parabolic equation at its vertex Z and Z is placed on the Y-th row and the X-th column pixel in $\mathbf{I}_{sort}$. Obviously, the value of Y is directly related to the center of the LED image. Calculating the average grayscale values on the i-th row, $m_i = E[g_{ij}]$, where g_{ij} denotes the grayscale value of the i-th row and the j-th column pixel in $\mathbf{I}$ and $1 \leq j \leq I_W$. Then,

$$Y = \arg\left\{\max_{1 \leq i \leq I_H} m_i\right\}. \tag{4}$$

After the parameters of X and p are chosen, the grayscale values $I_{sort}(x, y)$ of the coordinates (x, y) on the parabolic equation are selected to be $\mathbf{G}_s^{(\mathrm{P-CVS})}$, as a representation of the received DCO-OFDM signals.

The $\mathbf{G}_S$ selected by the method proposed in [11] and the $\mathbf{G}_s^{(\mathrm{P-CVS})}$ selected by the proposed P-CVS are depicted in Fig. 5. As can be seen in Fig. 5, the long-term variation of $\mathbf{G}_s$ is quite

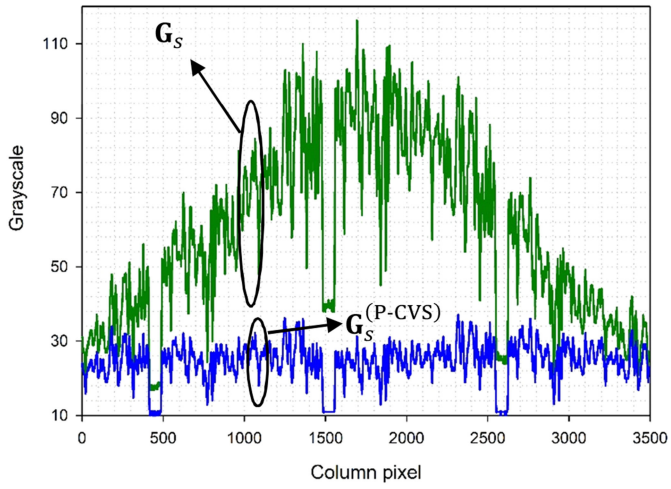

Fig. 5. Example results of the CVS in [11] and the proposed P-CVS method.

time-variant, and its variation is directly dependent on the intensity of the BEI. In other words, the grayscale values in $\mathbf{G}_s$ are not mainly related to $\mathbf{x}^{(\text{DCO})}$, and hence $\mathbf{G}_s$ is not suitable for DCO-OFDM signal demodulation. In contrast, the long-term variation of $\mathbf{G}_s^{(\text{P-CVS})}$ is less dependent on the BEI, making it suitable to serve as a replica of the transmitted $\mathbf{x}^{(\text{DCO})}$, in which it is denoted as $\breve{\mathbf{x}}^{(\text{DCO})}$ because it still contains the shot noise $\mathbf{n}_{shot}$.

3.2 The Decomposition of Extremely Low Frequency Component Algorithm

The pixels in $\mathbf{I}$ that are strongly interfered with by the BEI are almost saturated, and their grayscale values cannot represent the variation of the transmitted DCO-OFDM OCC signal. Meanwhile, the pixels in $\mathbf{I}$ that have insufficient exposure lack a sufficient amount of light to clearly record the transmitted signal variation. By using the rolling shutter, the recorded row-by-row grayscale values that are represented in (2) could be viewed as a time-domain signal, i.e., $I(i,j) = G_{og} \times G_{eo} \times x(i \cdot t_{expo}) \overset{\text{def}}{=} I(i \cdot t_{expo})$ without the consideration of the BEI and the shot noise. In fact, $I(i \cdot t_{expo})$ contains the BEI term $n_b(i,j)$, and traditionally, CVS-based methods were proposed to select $I(i,j)$ that would not be seriously distorted by the BEI, including the column vector selection with segmentation method [9], [10] and the column vector selection with image sorting and interpolation method [11], [12]. However, both can only be adopted in OOK OCC, whereas our proposed P-CVS method can be used in OFDM OCC. Moreover, the above-mentioned CVS-based methods only tried to reduce the influence of the BEI using time-domain signal processing, and neglected that the spectrum of $n_b(i,j)$ and $I(i \cdot t_{expo})$ can be separated.

In the DCO-OFDM OCC system, the intensity recorded in $\mathbf{I}$ comes from $\mathbf{x}^{(\text{DCO})}$, $\mathbf{n}_b$, and $\mathbf{n}_{shot}$, of which $\mathbf{n}_b$ is mainly caused by the driving current used to light up the LED. Most of the driving current is DC and can be viewed as an extremely low frequency signal that has a frequency spectrum that is lower than that of the transmitted DCO-OFDM signal. This motivated us to develop the decomposition of extremely low frequency component (D-ELFC) DCO-OFDM OCC signal detection without using column vector selection.

For each grayscale image $\mathbf{I}$, the average grayscale value on the i-th row, $m_i = E[g_{ij}]$, where g_{ij} denotes the grayscale value of the i-th row and the j-th column pixel in $\mathbf{I}$ and $1 \le j \le I_W$, is calculated. Let $\mathbf{G}_s^{(\text{D-ELFC})} = [m_1, m_2, \ldots, m_{I_H}]^T$ and use FFT on $\mathbf{G}_s^{(\text{D-ELFC})}$ to get its frequency-domain signal $\tilde{\mathbf{X}}^{(\text{DCO})}$, and its length and the sampling frequency are I_H and $f_{expo} = 1/t_{expo}$, respectively. In the D-ELFC method, the BEI is considered as an extremely low frequency signal. Hence, the BEI could

be reduced by passing $\tilde{\mathbf{X}}^{(\mathrm{DCO})}$ through a window function $\mathbf{W}_{n_b}$, defined as follows,

$$\mathbf{W}_{n_b}[i] = \begin{cases} 0, & 1 \le i \le n_b \\ 0, & I_H - (n_b - 2) < i \le I_H \\ 1, & \text{otherwise} \end{cases}, \tag{5}$$

where n_b denotes the cut-off frequency index. By eliminating the signal component whose spectrum frequency is lower than $n_b \times (f_{expo}/I_H)$, the reduced BEI time-domain signal after the D-ELFC method is $\breve{\mathbf{x}}^{(\mathrm{DCO})} = \mathrm{IFFT}(\tilde{\mathbf{X}}^{(\mathrm{DCO})} \times \mathbf{W}_{n_b})$.

3.3 Frequency-Domain Downsampling

The time-domain signal $\breve{\mathbf{x}}^{(\mathrm{DCO})}$ resulting from either the P-CVS method or the D-ELFC method is still affected by the shot noise, the bandwidth of which is wider than that of the transmitted DCO-OFDM signal. This motivate us to reduce the shot noise components contained in $\breve{\mathbf{x}}^{(\mathrm{DCO})}$ by eliminating the component of $\breve{\mathbf{x}}^{(\mathrm{DCO})}$ whose frequency is higher than that of $\mathbf{x}^{(\mathrm{DCO})}$, which would be accomplished by using the FDDS scheme. Suppose that the length of $\breve{\mathbf{x}}^{(\mathrm{DCO})}$ is U, and then use FFT on $\breve{\mathbf{x}}^{(\mathrm{DCO})}$, resulting in its frequency-domain signal $\breve{\mathbf{x}}^{(\mathrm{DCO})}$. The shot noise can be reduced by passing $\breve{\mathbf{x}}^{(\mathrm{DCO})}$ through a window function $\mathbf{W}_m$, defined as follows,

$$\mathbf{W}_m[i] = \begin{cases} 1, & 0 \le i \le (mN/2) + 1 \\ 1, & U - (mN/2) \le i < U - 1 \\ 0, & \text{otherwise} \end{cases}, \tag{6}$$

where N is the length of the transmitted signal $\mathbf{x}^{(\mathrm{DCO})}$ and m denotes the length of the resulting signal, which is m times the length of $\mathbf{x}^{(\mathrm{DCO})}$ after FDDS. Thus, $\overline{\mathbf{X}}^{(\mathrm{DCO})} = \breve{\mathbf{x}}^{(\mathrm{DCO})} \times \mathbf{W}_m$. IFFT is then used on $\overline{\mathbf{X}}^{(\mathrm{DCO})}$ to get the time-domain signal $\overline{\mathbf{X}}^{(\mathrm{DCO})}$, and the estimated DCO-OFDM signal $\hat{\mathbf{x}}^{(\mathrm{DCO})}[n]_{\downarrow m} = \overline{\mathbf{X}}^{(\mathrm{DCO})}[mn]$. For simplicity, this is denoted as m-FDDS. After demodulating $\hat{\mathbf{x}}^{(\mathrm{DCO})}[n]_{\downarrow m}$ to $\hat{\mathbf{X}} = [\hat{X}_0, \hat{X}_1, \ldots, \hat{X}_n, \ldots, \hat{X}_{N-1}]$, the M-ary QAM modulated symbol on each subcarrier could be de-mapped to logic values.

4. Experimental Setup and Results

The testbed setup of the DCO-OFDM OCC system is illustrated in Fig. 6. The pseudo-random binary sequence was programmed using MathWorks MATLAB on a computer, and was packetized as a combination of a 10-bit packet preamble by using OOK and a 128-bit data block with DCO-OFDM modulation. The DCO-OFDM modulation conducted $N = 128$ subcarriers, and each subcarrier adopted a 4-QAM signaling. To conduct the digital-to-analog conversion, the computer was connected to an arbitrary function generator (AFG3151C, Tektronix) for transmitting waveform generation with a data rate of R kbps with a 2.5-GHz sampling rate and a 14-bit resolution. The transmitted waveform was then superimposed on the DC bias current *a priori* to the intensity modulation of the adopted LED (Cree XPG2 R5). The dynamic range of the signal was set between 3 and 7 volts, and thus the worst peak-to-average power ratio (PAPR) was about 7.36 dB. The LED light source was located around the center of the CMOS image sensor, and the distance between the smartphone and the LED was assumed to be D, which was set between 15 cm and 30 cm to achieve the basic illuminance level in a typical office area. After free-space transmission, the modulated optical signal was received by a smartphone (ASUS ZE552KL) that has ISO 3200 and an exposure time of 1/13000. The captured photos, with 3492×4656 resolution, were processed using the open source computer vision library in C++ to restore the recorded images to the logic values by using the proposed methods, demodulation, and BER analysis.

In the P-CVS method, the position of the parabola vertex Z is located at (X, Y), where Y is calculated by (4) and the setting value of X is a system parameter. A smaller X could result in the

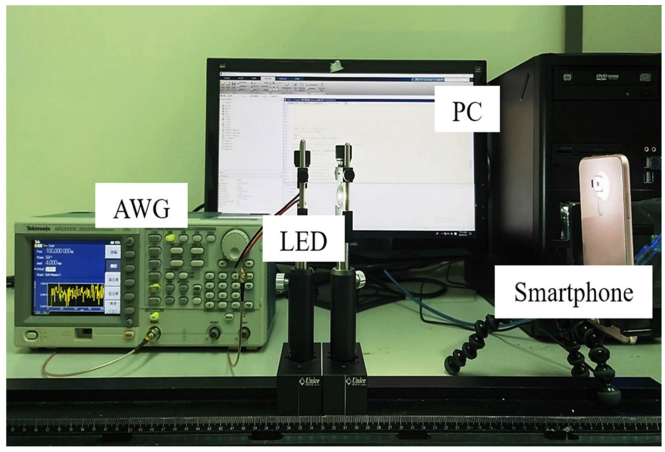

Fig. 6. System setup of the DCO-OFDM OCC testbed.

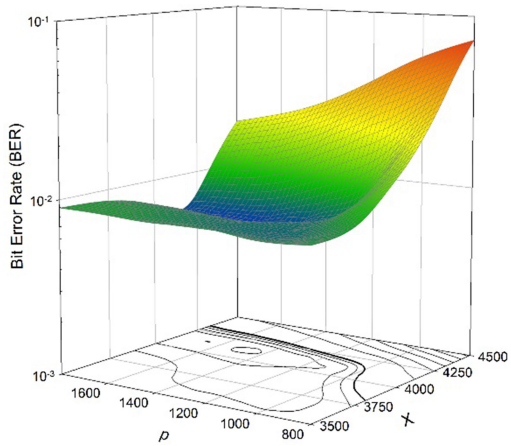

Fig. 7. BER versus different combinations of p and X for the P-CVS method when $D = 20$ cm and $R = 13.8$ kbps.

pixels value on P experiencing more serious BEI, while a larger X would make the pixels value on P have insufficient exposure to clearly record the transmitted signal variation. Moreover, the reciprocal of the parameter p in (3), i.e., $1/p$, represents the curvature of the parabolic equation, and a larger p gets a smaller curvature. To find the proper settings of X and p in the P-CVS method, Fig. 7 shows the bit error rate (BER) versus parameters X and p, in which $D = 20$ cm and $R = 13.8$ kbps. A smaller X causes the parabola to be closer to the region in $\mathbf{I}_{sort}$ that is seriously interfered with by the BEI, while a larger X causes the parabola to be closer to the region in $\mathbf{I}_{sort}$ with insufficient exposure. For the case of the adopted DCO-OFDM OCC testbed, the proper setting of X was around 4000, as shown in Fig. 7. Furthermore, the setting of $p = 1400$ resulted in the parabola having the proper curvature to get a $\mathbf{G}_s^{(\mathrm{P-CVS})}$ value that was almost independent of the BEI, as shown in Fig. 5. Fig. 8 shows the BERs of the P-CVS method versus the parameter m in the FDDS. On one hand, the BER of the P-CVS was apparently degraded due to undersampling when the 1-FDDS was used. On the other hand, much more shot noise would be introduced when adopting the 3-FDDS. For the case of this DCO-OFDM OCC system, the P-CVS method with 2-FDDS achieved the best BER of 6.627×10^{-3}.

To find the proper settings of the cut-off frequency index n_b and the m in the FDDS, the BER of the proposed D-ELFC method versus the combination of n_b and m are shown in Fig. 9, where

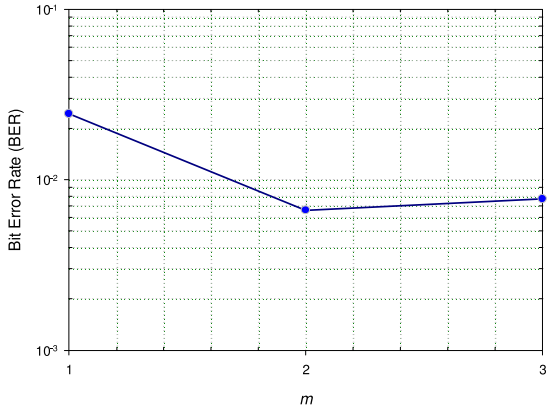

Fig. 8. BER versus the parameter m in the FDDS for the P-CVS method with $X = 4000$ and $p = 1400$ when $D = 20$ cm and $R = 13.8$ kbps.

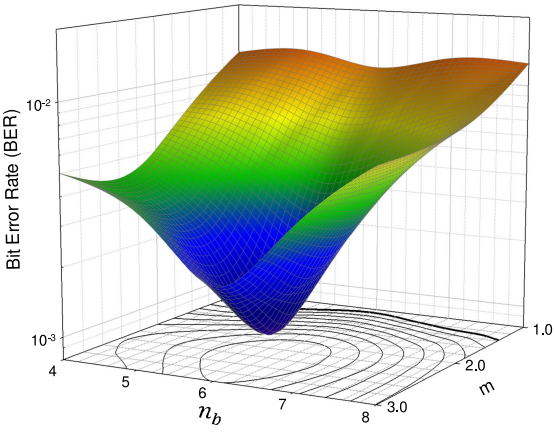

Fig. 9. BER versus different combinations of n_b and m for the D-ELFC method when $D = 20$ cm and $R = 13.8$ kbps.

$R = 13.8$ kbps and $D = 20$ cm. Generally, as can be seen in Fig. 9, the BER of the D-ELFC was decreased as n_b was increased. However, setting an excessive value of n_b would clip the original DCO-OFDM signals, resulting in BER degradation. As can be seen in Fig. 9, the adaptation of $n_b = 6$ with 2-FDDS was able to effectively eliminate the BEI and the shot noise, making the D-ELFC method reach its best BER performance of 1.763×10^{-3} for the case of $R = 13.8$ kbps and the distance between the LED and the smartphone being 20 cm.

Fig. 10 shows constellation diagrams of 4 QAM modulation under the condition that $D = 20$ cm and $R = 13.8$ kbps. As can be seen in Fig. 10, the constellation diagrams produced with the P-CVS method are more dispersed than those produced with the D-ELFC method. This observation was also validated by the error vector magnitude (EVM) results, which are shown in the titles of each subfigure. The measured BERs of the DCO-OFDM OCC with the P-CVS and the D-ELFC methods and the OOK OCC with the MEA [11] are presented in Fig. 11 for different transmission rates when $D = 20$ cm. As can be seen in Fig. 11, the BER of OCCs with the considered methods was degraded with increases in the data transmission rate. The BER performance of the OOK OCC is seriously deteriorated when the data rate is more than ten kbps. The performance of the DCO-OFDM OCC system is mainly limited by the exposure capability of the camera module. When the data transmission rate is increased, the signal variation between two successive exposure instants fluctuates, and thus the grayscale values recoded by the image sensor get more distorted

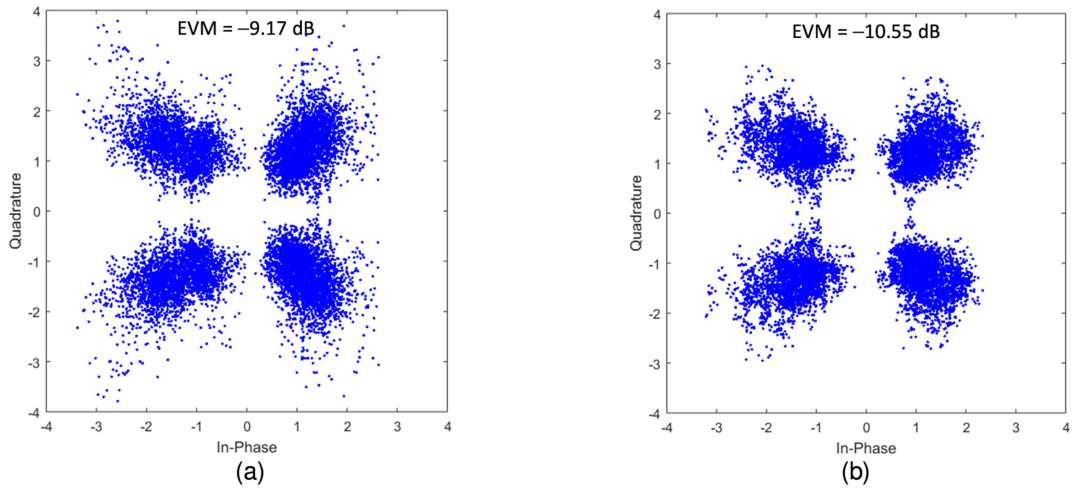

Fig. 10. Signal constellations of DCO-OFDM OCC when $D = 20$ cm and $R = 13.8$ kbps. (a) Using the P-CVS method. (b) Using the D-ELFC method.

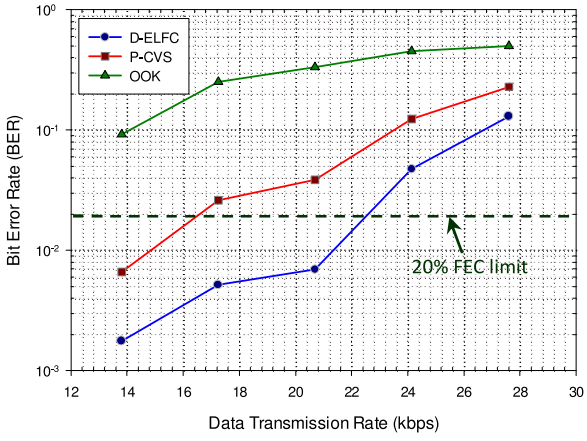

Fig. 11. BER versus the data transmission rate for the P-CVS method and the D-ELFC method when $D = 20$ cm, i.e., when the illuminance is around 510 lux.

in comparison to the original transmitted ones. Fortunately, this limitation might be overcome with advances in high-speed image sensors. Notably, the BER performance was substantially improved when using the proposed D-ELFC method in comparison to the results of the P-CVS method. This shows the superiority of the D-ELFC method that eliminates the BEI by using the principle of spectrum decomposition, whereas the P-CVS method only executes signal processing within the time-domain. Additionally, under the conditions of $D = 20$ cm, i.e., the illuminance being about 510 lux, and the BER being below the 20% forward error correction (FEC) limit, DCO-OFDM OCC with a data transmission rate $>$22 kbps can be achieved using the D-ELFC method with 2-FDDS.

Finally, the BERs of DCO-OFDM OCC with the P-CVS and the D-ELFC methods and the OOK OCC with the MEA [11] plotted against the distances between the LED and the smartphone for the case of $R = 13.8$ kbps are shown in Fig. 12. As can be seen in the figure, when the illuminance was over 220 lux, a BER below the 20% FEC limit could be achieved by using either the P-CVS method or the D-ELFC method, with 2-FDDS, while the BER performance of the OOK OCC was apparently worse than that of the DCO-OFDM OCC. In summary, the experimental results revealed that both the proposed P-CVS method and the proposed D-ELFC method could be used along with

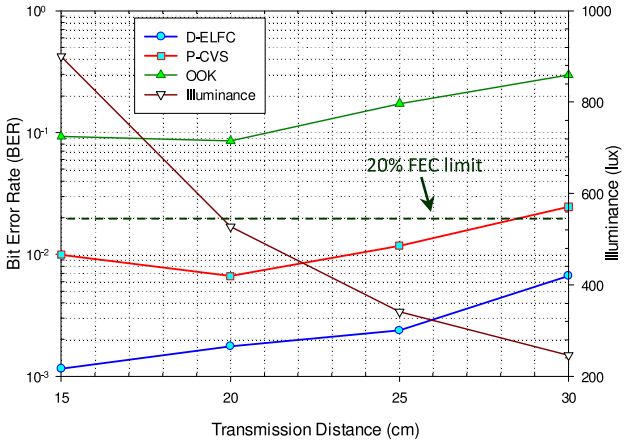

Fig. 12. BER versus the distance between the LED and the smartphone for the P-CVS method and the D-ELFC method when $R = 13.8$ kbps.

the 2-FDDS to achieve DCO-OFDM OCC systems. Additionally, the proposed D-ELFC method is capable of adequately reducing the BEI effect and, hence, of achieving better BER performance than the P-CVS scheme.

5. Conclusion

This study investigated the design and experimental implementation of the DCO-OFDM OCC system. Using a general commercial smartphone camera, a DCO-OFDM OCC testbed was successfully implemented to evaluate the proposed P-CVS algorithm and the proposed D-ELFC algorithm, along with the *m*-FDDS scheme. According to the experimental results, both the P-CVS algorithm and the D-ELFC algorithm were capable, along with the 2-FDDS, of demodulating the DCO-OFDM OCC signal. Moreover, the D-ELFC method, benefitting from the principle of spectrum decomposition, outperformed the P-CVS method, and a DCO-OFDM OCC with a data transmission rate up to 22 kbps was demonstrated to be achieved using the D-ELFC method under the 20% FEC limit.

References

[1] P. H. Pathak, X. Feng, P. Hu, and P. Mohapatra, "Visible light communication, networking, and sensing: A survey, potential and challenges," *IEEE Commun. Surveys Tut.*, vol. 17, no. 4, pp. 2047–2077, Fourth Quarter 2015.
[2] N. Ishikawa, S. Sugiura, and L. Hanzo, "50 years of permutation, spatial and index modulation: From classic RF to visible light communications and data storage," *IEEE Commun. Surveys Tut.*, vol. 20, no. 3, pp. 1905–1938, Third Quarter 2018.
[3] N. Saha, M. S. Ifthekhar, N. T. Le, and Y. M. Jang, "Survey on optical camera communications: Challenges and opportunities," *IET Optoelectronics*, vol. 9, no. 5, pp. 172–183, Oct. 2015.
[4] T. Nguyen, A. Islam, T. Hossan, and Y. M. Jang, "Current status and performance analysis of optical camera communication technologies for 5G networks," *IEEE Access*, vol. 5, pp. 4574–4594, Mar. 2017.
[5] *IEEE Standard for Local and Metropolitan Area Networks-Part 15.7: Short-Range Optical Wireless Communication*, IEEE Standards IEEE 802.15.7-2018, Dec. 2018.
[6] P. Ji, H. M. Tsai, C. Wang, and F. Liu, "Vehicular visible light communications with LED taillight and rolling shutter camera," in *Proc. IEEE Veh. Technol. Conf. Spring*, 2014, pp. 1–6.
[7] W. Huang, P. Tian, and Z. Xu, "Design and implementation of a real-time CIM-MIMO optical camera communication system," *Opt. Exp.*, vol. 24, pp. 24567–24579, 2016.
[8] V. P. Rachim and W. Chung, "Multilevel intensity-modulation for rolling shutter-based optical camera communication," *IEEE Photon. Technol. Lett.*, vol. 30, no. 10, pp. 903–906, May 2018.
[9] C. Chow, Y. Liu, R. Shiu, and C. Yeh, "Adaptive thresholding scheme for demodulation of rolling-shutter images obtained in CMOS image sensor based visible light communications," *IEEE Photon. J.*, vol. 10, no. 6, Dec. 2018, Art. no. 7908506.
[10] C. W. Chow, C. Y. Chen, and S. H. Chen, "Enhancement of signal performance in LED visible light communications using mobile phone camera," *IEEE Photon. J.*, vol. 7, no. 5, Oct. 2015, Art no. 7903607.

[11] Z. Zhang, T. Zhang, J. Zhou, Y. Qiao, A. Yang, and Y. Lu, "Performance enhancement scheme for mobile-phone based VLC using moving exponent average algorithm," *IEEE Photon. J.*, vol. 9, no. 2, Apr. 2017, Art. no. 7903207.
[12] Z. Zhang, T. Zhang, X. Tang, Y. Lu, and Y. Qiao, "Reducing grayscale value fluctuation for mobile-phone camera based VLC system," *IEEE Photon. J.*, vol. 10, no. 6, Dec. 2018, Art. no. 7908010.
[13] T. Nguyen, M. D. Thieu, and Y. M. Jang, "2D-OFDM for optical camera communication: Principle and implementation," *IEEE Access*, vol. 7, pp. 29405–29424, Feb. 2019.
[14] W. Chujo and M. Kinoshita, "Rolling-shutter-based QPSK by spatial luminance distribution for optical camera communication," in *Proc. IEEE Globecom Workshops (GC Wkshps)*, Abu Dhabi, United Arab Emirates, 2018, pp. 1–6.
[15] H. Nguyen, M. D. Thieu, T. Nguyen, and Y. M. Jang, "Rolling OFDM for image sensor based optical wireless communication," *IEEE Photon. J.*, vol. 11, no. 4, Aug. 2019, Art. no. 6500817.
[16] Y. Goto *et al.*, "A new automotive VLC system using optical communication image sensor," *IEEE Photo. J.*, vol. 8, no. 3, Jun. 2016, Art. no. 6802716.
[17] D. J. F. Barros, S. K. Wilson, and J. M. Kahn, "Comparison of orthogonal frequency-division multiplexing and pulse-amplitude modulation in indoor optical wireless links," *IEEE Trans. Commun.*, vol. 60, no. 1, pp. 153–163, Jan. 2012.
[18] O. Gonzalez, R. Perez-Jimenez, S. Rodriguez, J. Rabadan, and A. Ayala, "Adaptive OFDM system for communications over the indoor wireless optical channel," *IET Proc. Optoelectronics*, vol. 153, pp. 139–144, 2006.
[19] J. Armstrong and A. J. Lowery, "Power efficient optical OFDM," *Electron. Lett.*, vol. 42, pp. 370–372, 2006.
[20] J. M. Kahn and J. R. Barry, "Wireless infrared communications," *Proc. IEEE*, vol. 85, no. 2, pp. 265–298, Feb. 1997.